Angewandte Chemie

Akzeptierter Artikel

Single-Nanoparticle Cell Barcoding by Tunable FRET from Lanthanides to Quantum Dots

Chi Chen[1], Lijiao Ao[3], Yu-Tang Wu[1], Vjona Cifliku[1], Marcelina Cardoso Dos Santos[1], Emmanuel Bourrier[4], Martina Delbianco[5,6], David Parker[5], Jurriaan M. Zwier[4], Liang Huang[2]*, Niko Hildebrandt[1]*

[1] NanoBioPhotonics (nanofret.com), Institute for Integrative Biology of the Cell (I2BC), Université Paris-Saclay, Université Paris-Sud, CNRS, CEA, 91400 Orsay, France. [2] College of Chemical Engineering, Zhejiang University of Technology, 310014, Hangzhou, P.R. China. [3] Institute of Biomedicine and Biotechnology, Shenzhen Institutes of Advanced Technology, Chinese Academy of Sciences, 518055, Shenzhen, P.R. China. [c] Cisbio Bioassays, Parc Marcel Boiteux, BP 84175, Condolet, France. [5] Department of Chemistry, Durham University, South Road, DH13LE, Durham, United Kingdom. [6] Current affiliation: Max Planck Institute of Colloids and Interfaces, Potsdam, Germany.

* Corresponding authors: *lhuang@zjut.edu.cn,* niko.hildebrandt@u-psud.fr

***Keywords:*** *FRET, Lanthanides, Quantum Dots, Lifetime, Imaging*

Supporting Information for this article is available on the WWW under…

ABSTRACT: Fluorescence barcoding based on nanoparticles provides many advantages for multiparameter imaging. However, creating different concentration-independent codes without mixing various nanoparticles and by using single wavelength excitation and emission for multiplexed cellular imaging is extremely challenging. Here, we report the development of quantum dots (QDs) with two different SiO_2 shell thicknesses (6 and 12 nm) and coated with two different lanthanide complexes (Tb and Eu). FRET from Tb or Eu donors to the QD acceptors resulted in four distinct photoluminescence (PL) decays, which were encoded by simple time-gated (TG) PL intensity detection in three individual temporal detection windows. The well-defined single-nanoparticle codes were used for live cell imaging and a one-measurement distinction of four different cells in a single field of view. This single-color barcoding strategy opens new opportunities for multiplexed labeling and tracking of cells.

Optical encoding has great potential for nanomedicine, diagnostics, biosensing, document security, and optical data storage.[1–4] Such barcoding has exploited both the emission color[1,5] and the excited-state lifetime[6–8] components of PL. The majority of encoding approaches applied mixing of different luminescent molecules or nanoparticles in microspheres[1,6,7] or cells.[5,8,9] Using individual dyes or nanoparticles (e.g., QDs)[10,11] for optical encoding is limited by the spectral overlap of their PL spectra and the concentration-dependence of PL intensity. Concentration-independent PL lifetime-multiplexing with individual nanoparticles has also been demonstrated. One concept used upconversion nanoparticles (UCNPs) with varying co-doping concentrations of Yb^{3+} and Tm^{3+} ions, but only for proof-of-concept biosensing and security printing,[2] most probably due to the limited brightness of UCNPs.[12] Individual QDs were also used for PL lifetime tuning through bandgap engineering, including increasing the particle size,[13] introducing various dopants,[7,14] and fabricating the nanostructure with lattice-strain.[8,15] Unfortunately, these methods led to the change of PL wavelengths and thus, color could not be used as an independent parameter, which is a prerequisite for combining both color and lifetime into higher-order multiplexing. A facile and robust strategy to prepare lifetime-tunable QDs that are independent of PL color would significantly advance this endeavor.

Förster resonance energy transfer (FRET) is a strongly distance-dependent interaction within a luminescent donor-acceptor pair and the donor-acceptor distance defines the PL lifetime of the donor.[16] A FRET pair of lanthanide (e.g., Eu^{3+} or Tb^{3+}) donors and QD acceptors is of particular interest for multiplexed biosensing, because lanthanides possess very long PL lifetimes and QDs provide color-tunability and narrow PL emission.[17–20] Due to the large difference between the PL lifetimes of lanthanides (~ms) and QDs (~ns), the FRET-sensitized lifetime of the QD acceptor is the same as the FRET-quenched lifetime of the lanthanide donor.[19] Therefore, shorter (or longer) lanthanide-QD distances lead to shorter (or longer) PL lifetimes of both lanthanide and QD. We have recently shown that a single Tb-QD FRET pair can be used for TG detection of multiple miRNAs by PL lifetime tuning via Tb-to-QD distance adjustment.[21] Here, we demonstrate that such a distance tuning approach can be used within one single nanoparticle by direct attachment of the lanthanides to QD-coatings with different thicknesses and that these individual lanthanide-coated QD nanohybrids can be used for encoding of different cells via TG temporal multiplexing.
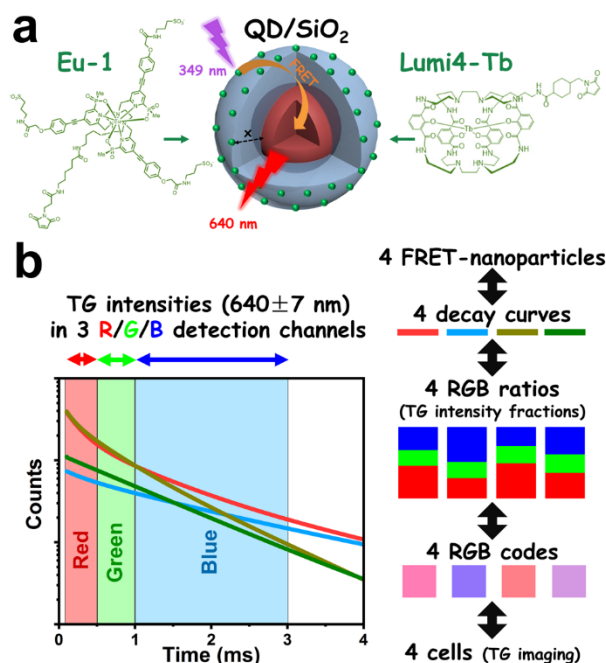
Scheme 1. (a) QDs with SiO_2-coatings of different thicknesses (x = 6 or 12 nm) functionalized with Eu-1 or Lumi4-Tb for single-wavelength temporal PL barcoding. (b) RGB encoding principle based on three distinct TG PL intensity fractions for each of the four FRET-specific PL decays (see Figure 1 for technical details).

Table 1. Optical Characteristics of Tb, Eu, and QD/SiO$_2$ with Their FRET Pairs.

	ε_{max} (M^{-1} cm^{-1}) [λ_{max}]	Φ_{Ln3+}	Emission Filter (nm)[a]	τ[b]
Lumi4-Tb	26,000 [340 nm]	0.79	490/20	2.7 ms
Eu-1	58,000 [330 nm]	0.48	567/15	1.1 ms
QD/SiO$_2$ (6 nm)	599,500 [610 nm]	/	640/14	~12 ns
QD/SiO$_2$ (12 nm)	1,770,000 [610 nm]	/	640/14	~11 ns
FRET pair (D → A)	J (M^{-1}. cm^{-1}. nm^4)	R_0 (nm)		τ_{ave} (ms)[c]
Tb → QD/SiO$_2$(6 nm)	8.5×10^{16}	10.3		0.74
Tb → QD/SiO$_2$(12 nm)	2.4×10^{17}	12.2		1.82
Eu → QD/SiO$_2$(6 nm)	7.2×10^{16}	9.2		0.61
Eu → QD/SiO$_2$(12 nm)	2.3×10^{17}	11.1		1.09

(a) See **Figure S6** for filter spectra. Lumi4-Tb and Eu-1 filters were selected to measure their bluest emission bands with the least possible overlap with the QD emission band. QD filter was selected to avoid overlap with Tb and Eu PL. (b) See **Figure S7** for PL decay curves. (c) Amplitude averaged decay time that takes into account the complete decay curves, which contain FRET-quenched and unquenched (lanthanide complexes that do not participate in FRET) components. FRET-quenched average decay times, FRET efficiencies, and donor-acceptor distances can be found in **Table S1**.

As a prototypical system for FRET lifetime encoding via individual nanoparticles (**Scheme 1**), we used silica as transparent and controllable coating matrix for QDs (CdSe/CdS/ZnS, emission maximum at 620 nm).[22,23] The QDs were coated with size-controlled (6 and 12 m) and uniform thiol-functionalized silica shells (QD-SiO$_2$), to which two different maleimide-functionalized lanthanide complexes (Lumi4-Tb and Eu-1)[24–26] were conjugated.
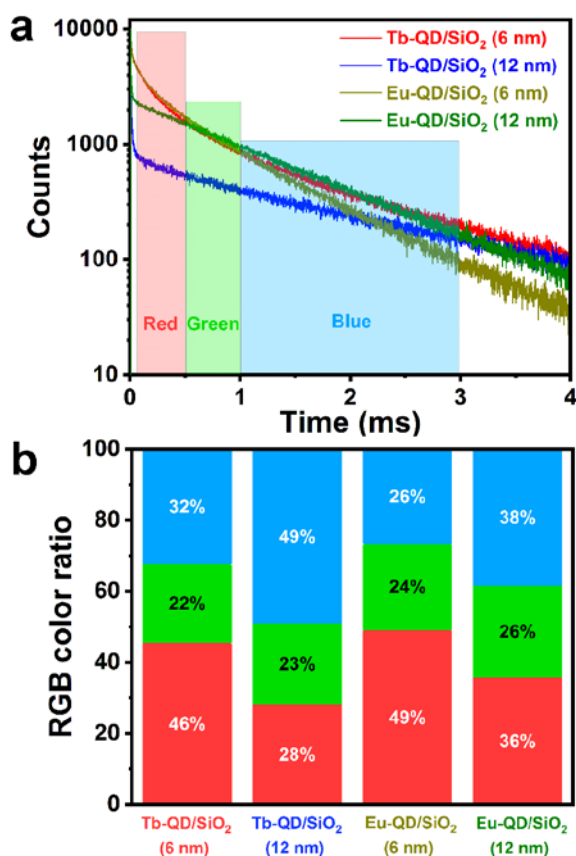

Figure 1. (a) QD acceptor PL decay curves of each single nanoparticle code. (b) TG PL intensity (RGB) ratio of each single nanoparticle code calculated from the TG intensities in the red, green, and blue TG detection windows in a.

High resolution transmission electron microscopy (HRTEM, **Figure S1**) showed nearly monodisperse QDs with clearly defined SiO$_2$ nanoshells of 6 nm and 12 nm thicknesses. Absorption and emission spectra of Lumi4-Tb, Eu-1, QD, QD/SiO$_2$(6 nm) and QD/SiO$_2$(12 nm) are presented in **Figure S2**. Both lanthanide complexes were excitable in the 300 to 400 nm wavelength region and their PL spectra overlapped well with the QD absorption spectra for efficient FRET (**Figure S3**). Photophysical and FRET parameters for the different single luminophores and the donor-acceptor combinations are listed in **Table 1**. Although the PL emission wavelength of QDs before and after SiO$_2$ coating did not change (**Figure S2**), the extinction coefficient of QD/SiO$_2$ significantly increased with increasing shell thickness due to a better protection of the QD from the environment. The spectral overlap integral (J) and Förster distance (R_0) of each individual FRET-pair were calculated. UV-vis absorbance spectra were employed to calculate the number of lanthanide donors per QD acceptor. The absorbance spectra (**Figure S4**), which presented linear combinations of QD-SiO$_2$ and the lanthanide complexes, resulted in labeling ratios of ~75 Lumi4-Tb per QD/SiO$_2$(6 nm), ~87 Lumi4-Tb per QD/SiO$_2$(12 nm), ~175 Eu-1 per QD/SiO$_2$(6 nm), and ~180 Eu-1 per QD/SiO$_2$(12 nm). Approximate double amounts for Eu-1 were used to account for the lower brightness (lower extinction coefficient at the microscopy excitation wavelength of 349 nm and lower quantum yield) of Eu-1 compared to Lumi4-Tb. Due to the long PL lifetime of lanthanides, one QD can be sensitized by FRET from several lanthanide donors and therefore an increasing number of donors increases the overall brightness of FRET-sensitized QD emission.

Due to the different distances (6 nm or 12 nm) and different R_0 values (between 9.2 and 12.2 nm, **Table 1**), the PL lifetimes (τ) of Lumi4-Tb (2.7 ms) and Eu-1(1.1 ms) were quenched to different extents. Because of the much shorter PL lifetime of the QDs (ns) compared to the lanthanide complexes (ms), the FRET-quenched PL decay times of the lanthanides equaled the FRET-sensitized PL decay times of the QDs.[17] Therefore, FRET led to distinct and long-lived QD decays (**Figure 1a** and **Figure S5**) with average decay times (τ_{ave}) between 0.61 ms and 1.82 ms (**Table 1**) for the four lanthanide-QD FRET nanoparticles. Steady-state PL spectra also showed increased lanthanide PL quenching with decreasing shell thickness (**Figure S6**). Based on the PL decay curves, we also calculated FRET efficiencies and

donor acceptor distances (Tb/Eu-to-QD distances of 8.0 nm / 8.3 nm for the 6 nm SiO_2 shell and 11.3 nm /12.5 nm for the 12 nm SiO_2 shell), which were in very good agreement with the QD-SiO_2 structures and distances from HRTEM (**Figure S1**), taking into account the random conjugation of the lanthanide complexes on the surface of the SiO_2 shell.
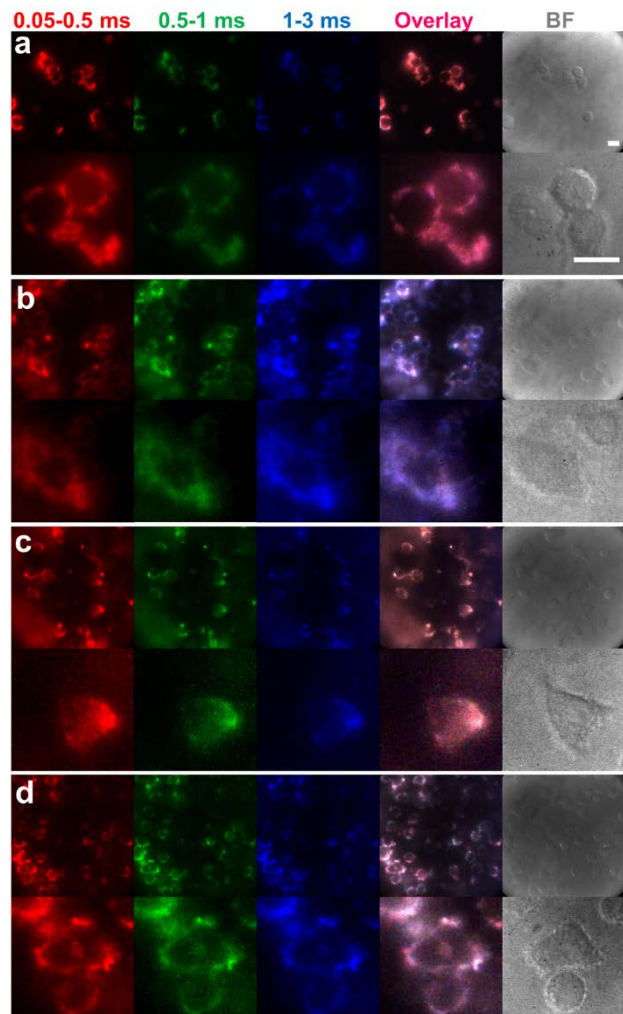

Figure 2. TG PL images (top panels) and high resolution TG PL images (bottom panels) in different temporal detection windows (time-ranges on top), their overlay, and bright field (BF) images of HeLa cells labeled with individual nanoparticle codes. (a) Tb-QD/SiO$_2$(6 nm), (b) Tb-QD/SiO$_2$(12 nm), (c) Eu-QD/SiO$_2$(6 nm), (d) Eu-QD/SiO$_2$(12 nm). Scale bar (top right): 20 μm; λ_{ex}: 349 nm; λ_{em}: 640 nm.

The principle of TG RGB encoding is illustrated in **Scheme 1b**. Based on the intersections of the four distinct PL decay curves (**Figure 1a**), three temporally distinct TG PL intensity detection windows were selected and defined as red (R), green (G), and blue (B), respectively. One PL intensity (integrated over the time interval of the detection channel) is recorded for each channel. The different shapes of the decay curves (different PL lifetimes) result in distinct PL intensity combinations of the three detection channels R, G, and B. Thereby, each FRET-nanoparticle can be identified by a unique RGB ratio (ratios of TG PL intensities: R/(R+G+B), G/(R+G+B), and B/(R+G+B); **Figure 1b** and **Table S2**). TG imaging uses the same three TG detection windows as defined by the decay curves and each camera pixel records three time-dependent intensities (R, G, and B) for each image. *ImageJ* was used to assign red, green, or blue color to the three detection channels and define a common intensity range (same minimum and maximum values for all channels). The resulting overlay images provide RGB codes (between 0 and 255 for R, G, and B) for each pixel, which can then be

transferred into RGB ratios and directly related to the four different FRET-nanoparticles. As a first evaluation of biocompatibility, the stability of the RGB codes was analyzed for the four different nanoparticles incubated in PBS buffer at different pH (5.3, 6.8, and 7.5) for 2h and 4h. TG PL intensity ratios of each code were nearly invariant (**Figure S8**), which provided first good evidence concerning compatibility of our temporal PL encoding approach with live cell imaging.

To demonstrate the actual application for live cell imaging, HeLa cells were incubated with Tb-QD/SiO$_2$(6 nm), Tb-QD/SiO$_2$(12 nm), Eu-QD/SiO$_2$(6 nm), and Eu-QD/SiO$_2$(12 nm), respectively. Although adequately coated and biocompatible QDs have been used in many biological imaging applications in vivo and in vitro, their toxicity remains an important subject of discussion.[11] Cell viability tests (MTT assays) with QD concentrations up to 800 nM (the concentration used for imaging experiments was only 20 nM) for both QD/SiO$_2$(6 nm) and QD/SiO$_2$(12 nm) revealed no significant cytotoxicity (**Figure S9**). To encode the cells incubated with a specific nanoparticle, we used a TG microscopy imaging system with pulsed laser excitation at 349 nm and time-gated detection of the QD PL by an intensified CCD camera.[27] In general, TG microscopy in the micro and millisecond range can be realized on any standard fluorescence microscope that is equipped with pulsed excitation (e.g., LEDs, lasers, flash lamps, mechanical choppers) and time-gated detection (e.g., intensified cameras, scanning photon detectors, mechanical choppers).[28,29] As defined before in the PL decay experiments, TG windows of 0.05-0.5 ms (R), 0.5-1 ms (G), and 1-3 ms (B) were selected for TG image encoding (**Figure 2**). After merging the images from the three TG detection windows (overlay), the RGB color images were obtained. Each code was determined according to RGB color selection and was consistent with the previously calculated results obtained by PL decays. Noteworthy, the different RGB colors could be readily distinguished by the naked eye (**Figure 2**).
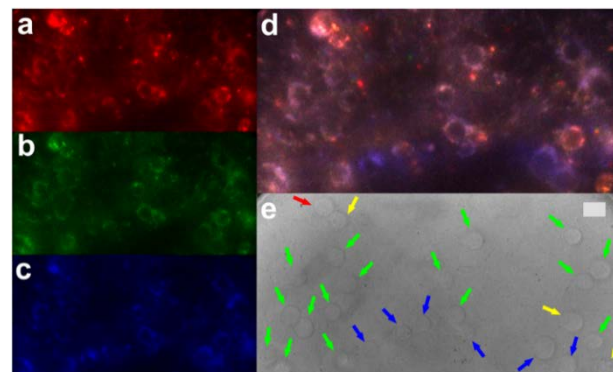

Figure 3. TG PL images of differently encoded HeLa cells. (a) 0.05-0.5 ms; (b) 0.5-1 ms; (c) 1-3 ms; (d) overlay; (e) bright field - red arrow: Tb-QD/SiO$_2$(6 nm), blue arrows: Tb-QD/SiO$_2$(12 nm), yellow arrows: Eu-QD/SiO$_2$(6 nm), green arrows: Eu-QD/SiO$_2$(12 nm). Scale bar (in e): 20 μm; λ_{ex}: 349 nm; λ_{em}: 640 nm.

To emphasize the capability of these codes to distinguish cells in more complex environments, four differently encoded HeLa cells were mixed and cultured on the same microscopy slide. As shown in **Figure 3**, single-color (one excitation and one emission wavelength) TG imaging could efficiently distinguish the four types of cells within the same field of view. Again, the four RGB codes can be already distinguished by the naked eye (**Figure 3d**). However, for clarity and taking into account the different color impressions from screen to screen and from screen to paper, we retrieved the RGB codes from color selection within the overlay image and marked the different cells with colored arrows in the bright field images (**Figure 3e**). We noted that the RGB color of each code in this rather complex mixing envi-

ronment exhibited less blue, which we assigned to quenching effects during the 8 h incubation time. Still, we could clearly distinguish the encoded cells via the ratios of TG PL intensities. Finally, to demonstrate the independence of PL intensity and probe concentration, different encoding nanoparticles were incubated at distinct concentration with HeLa cells and afterwards the cells were mixed. Adjusting brightness and contrast within the same field of view also allowed us to distinguish cells with significantly different PL intensities (**Figure S10**).

In summary, we have developed and applied a single-wavelength, single-nanoparticle encoding system composed of QD cores with lanthanide-functionalized SiO_2 shells. Our TG-FRET barcoding technique was accomplished by precise distance control between lanthanide donors and QD acceptors, which, in turn, led to distinct PL decay curves. TG PL detection in three specific time windows allowed us to create distinct RGB codes for each encoding nanoparticle, which were used to label live cells. Individual and mixed cells could be distinguished by the predefined RGB codes in the same field of view using TG PL imaging. Our encoding approach was independent of PL intensity and nanoparticle concentration and was shown to be stable at different pH over several hours of incubation. While our study used two different QD coating thicknesses and two different lanthanide complexes to create four different codes, more variations could be used to extend the coding range by additional lifetimes. Although a larger lifetime difference will always lead to a better distinction, the curves of Eu-QD/SiO_2(6 nm) and Tb-QD/SiO_2(6 nm) are very similar with an average lifetime difference of only ca. 20% (0.61 and 0.74 ms, cf. **Table 1**) but can still be distinguished very efficiently. A 20% difference between all lifetimes and a minimum lifetime of ca. 10 % of the one of Lumi4-Tb (2.7 ms) would allow for 14 different codes (lifetimes of 0.25, 0.30, 0.36, 0.44, 0.52, 0.63, 0.75, 0.90, 1.09, 1.30, 1.56, 1.88, 2.25, and 2.70 ms). If the coding system of interest requires more than 20% lifetime difference, the FRET multiplexing range can be extended by other means, e.g., by a combination of the spectral and temporal multiplexing components or by multistep FRET processes, in which the QD is used both as acceptor (to a Tb complex) and donor (to a dye). Such approaches have already been used in solution to quantify multiple DNAs by spectrotemporal multiplexing[30] or for the design of sophisticated molecular logic gates[31,32] Taking into account that lanthanide-to-QD FRET can be applied to many different QD colors,[18,33–35] our single nanoparticle encoding strategy shows the potential of extending to higher-order spectrotemporal PL barcoding and thereby significantly advancing the possibilities of fluorescent encoding.

ACKNOWLEDGMENT

REFERENCES

[1] M. Han, X. Gao, J. Z. Su, S. Nie, *Nat. Biotechnol.* **2001**, *19*, 631–635.
[2] Y. Lu, J. Zhao, R. Zhang, Y. Liu, D. Liu, E. M. Goldys, X. Yang, P. Xi, A. Sunna, J. Lu, et al., *Nat. Photonics* **2014**, *8*, 32–36.
[3] P. Zijlstra, J. W. M. Chon, M. Gu, *Nature* **2009**, *459*, 410–413.
[4] Y. Leng, K. Sun, X. Chen, W. Li, *Chem. Soc. Rev.* **2015**, *44*, 5552–5595.
[5] B. Andreiuk, A. Reisch, M. Lindecker, G. Follain, N. Peyriéras, J. G. Goetz, A. S. Klymchenko, *Small* **2017**, *13*, 1701582.
[6] Y. Lu, J. Lu, J. Zhao, J. Cusido, F. M. Raymo, J. Yuan, S. Yang, R. C. Leif, Y. Huo, J. A. Piper, et al., *Nat. Commun.* **2014**, *5*, 3741.
[7] C. Chen, P. Zhang, G. Gao, D. Gao, Y. Yang, H. Liu, Y. Wang, P. Gong, L. Cai, *Adv. Mater.* **2014**, *26*, 6313–6317.
[8] L. Zhang, C. Chen, W. Li, G. Gao, P. Gong, L. Cai, *ACS Appl. Mater. Interfaces* **2016**, *8*, 13187–13191.
[9] P. Rees, J. W. Wills, M. R. Brown, J. Tonkin, M. D. Holton, N. Hondow, A. P. Brown, R. Brydson, V. Millar, A. E. Carpenter, et al., *Nat. Methods* **2014**, *11*, 1177–1181.
[10] T. L. Jennings, S. G. Becker-Catania, R. C. Triulzi, G. Tao, B. Scott, K. E. Sapsford, S. Spindel, E. Oh, V. Jain, J. B. Delehanty, et al., *ACS Nano* **2011**, *5*, 5579–5593.
[11] K. D. Wegner, N. Hildebrandt, *Chem. Soc. Rev.* **2015**, *44*, 4792–4834.
[12] H. H. Gorris, O. S. Wolfbeis, *Angew. Chemie - Int. Ed.* **2013**, *52*, 3584–3600.
[13] A. L. Rogach, T. Franzl, T. A. Klar, J. Feldmann, N. Gaponik, V. Lesnyak, A. Shavel, A. Eychmuller, Y. P. Rakovich, J. F. Donegan, *J. Phys. Chem. C* **2007**, *111*, 14628–14637.
[14] C. Chen, P. Zhang, L. Zhang, D. Gao, G. Gao, Y. Yang, W. Li, P. Gong, L. Cai, *Chem. Commun.* **2015**, *51*, 11162–11165.
[15] A. M. Smith, A. M. Mohs, S. Nie, *Nat. Nanotechnol.* **2009**, *4*, 56–63.
[16] I. Medintz, N. Hildebrandt, *FRET – Förster Resonance Energy Transfer: From Theory to Applications*, Wiley-VCH Verlag GmbH And Co. KGaA, Weinheim, Ed. 1, **2013**.
[17] N. Hildebrandt, C. M. Spillmann, W. R. Algar, T. Pons, M. H. Stewart, E. Oh, K. Susumu, S. A. Díaz, J. B. Delehanty, I. L. Medintz, *Chem. Rev.* **2017**, *117*, 537–711.
[18] M. Cardoso Dos Santos, N. Hildebrandt, *TrAC - Trends Anal. Chem.* **2016**, *84*, 60–71.
[19] N. Hildebrandt, K. D. Wegner, W. R. Algar, *Coord. Chem. Rev.* **2014**, *273–274*, 125–138.
[20] O. Faklaris, M. Cottet, A. Falco, B. Villier, M. Laget, J. M. Zwier, E. Trinquet, B. Mouillac, J. P. Pin, T. Durroux, *FASEB J.* **2015**, *29*, 2235–2246.
[21] X. Qiu, J. Guo, Z. Jin, A. Petreto, I. L. Medintz, N. Hildebrandt, *Small* **2017**, *13*, 1700332.
[22] B. Ji, E. Giovanelli, B. Habert, P. Spinicelli, M. Nasilowski, X. Xu, N. Lequeux, J. Hugonin, F. Marquier, J. Greffet, et al., *Nat. Nanotechnol.* **2015**, *10*, 170–175.
[23] L. Huang, T. Liao, J. Wang, L. Ao, W. Su, J. Hu, *Adv. Funct. Mater.* **2018**, *28*, 1705380.
[24] J. Xu, T. M. Corneillie, E. G. Moore, G. L. Law, N. G. Butlin, K. N. Raymond, *J. Am. Chem. Soc.* **2011**, *133*, 19900–19910.
[25] M. Delbianco, V. Sadovnikova, E. Bourrier, G. Mathis, L. Lamarque, J. M. Zwier, D. Parker, *Angew. Chemie - Int. Ed.* **2014**, *53*, 10718–10722.
[26] S. J. Butler, M. Delbianco, L. Lamarque, B. K. McMahon, E. R. Neil, R. Pal, D. Parker, J. W. Walton, J. M. Zwier, *Dalt. Trans.* **2015**, *44*, 4791–4803.
[27] M. Cardoso Dos Santos, J. Goetz, H. Bartenlian, K.-L. Wong, L. J. Charbonnière, N. Hildebrandt, *Bioconjug. Chem.* **2018**, *29*, 1327–1334.
[28] N. Gahlaut, L. W. Miller, in *Cytom. Part A*, **2010**, pp. 1113–1125.
[29] J. M. Zwier, N. Hildebrandt, in *Rev. Fluoresc. 2016* (Ed.: C.D. Geddes), Springer, **2017**, pp. 17–43.
[30] X. Qiu, J. Guo, J. Xu, N. Hildebrandt, *J. Phys. Chem. Lett.* **2018**, *9*, 4379–4384.
[31] J. C. Claussen, N. Hildebrandt, K. Susumu, M. G. Ancona, I. L. Medintz, *ACS Appl. Mater. Interfaces* **2014**, *6*, 3771–3778.
[32] J. C. Claussen, W. R. Algar, N. Hildebrandt, K. Susumu, M. G. Ancona, I. L. Medintz, *Nanoscale* **2013**, *5*, 12156–12170.
[33] X. Qiu, N. Hildebrandt, *ACS Nano* **2015**, *9*, 8449–8457.
[34] D. Geißler, L. J. Charbonnière, R. F. Ziessel, N. G. Butlin, H. G. Löhmannsröben, N. Hildebrandt, *Angew. Chemie - Int. Ed.* **2010**, *49*, 1396–1401.
[35] F. Morgner, D. Geißler, S. Stufler, N. G. Butlin, H. G. Löhmannsröben, N. Hildebrandt, *Angew. Chemie - Int. Ed.* **2010**, *49*, 7570–7574.